

# Image-Based Acquisition and Modeling of Polarimetric Reflectance

## Supplemental Material #1

SEUNG-HWAN BAEK, KAIST  
TIZIAN ZELTNER, EPFL  
HYUN JIN KU and INSEUNG HWANG, KAIST  
XIN TONG, Microsoft Research Asia  
WENZEL JAKOB, EPFL  
MIN H. KIM, KAIST

### ACM Reference Format:

Seung-Hwan Baek, Tizian Zeltner, Hyun Jin Ku, Inseung Hwang, Xin Tong, Wenzel Jakob, and Min H. Kim. 2020. Image-Based Acquisition and Modeling of Polarimetric Reflectance: Supplemental Material #1. *ACM Trans. Graph.* 39, 4, Article 1 (July 2020), 3 pages. <https://doi.org/10.1145/3386569.3392387>

In this supplemental document, we provide details of system components, validation, tabulation, additional results, and pBRDF fitting.

## 1 SYSTEM COMPONENTS

We built our image-based pBRDF acquisition setup with various optical and mechanical components. Table 1 provides complete list of every part used in our system. In particular, the achromatic retarder is one of the most crucial components in our setup to acquire accurate polarimetric measurements across visible wavelengths. From tests of many retarders, we chose an achromatic retarder, Thorlabs AQWP10M-580. Figure 1 shows the actual retardance of the achromatic retarder that has a small deviation from the ideal retardance. This gap between the real and ideal retardance is handled by our linear reconstruction method described in Section 5.4 in the main paper.

## 2 SYSTEM VALIDATION ON BASIC SAMPLES

To validate the accuracy of polarimetric calibration and Muller matrix reconstruction, we captured and reconstructed the Mueller matrices of optical elements: horizontal and vertical linear polarizers, and circular polarizers with counter-clockwise rotation and clockwise rotation. Figure 2 shows the estimated Mueller matrices compared with the ideal Mueller matrices of the components.

---

Authors' addresses: Seung-Hwan Baek, KAIST, School of Computing, Daejeon, South Korea, 34141; Tizian Zeltner, EPFL, , Hyun Jin Ku; Inseung Hwang, KAIST, School of Computing, Daejeon, South Korea, 34141; Xin Tong, Microsoft Research Asia, Wenzel Jakob, EPFL, , Min H. Kim, KAIST, School of Computing, Daejeon, South Korea, 34141, [minhkim@kaist.ac.kr](mailto:minhkim@kaist.ac.kr).

---

Permission to make digital or hard copies of part or all of this work for personal or classroom use is granted without fee provided that copies are not made or distributed for profit or commercial advantage and that copies bear this notice and the full citation on the first page. Copyrights for third-party components of this work must be honored. For all other uses, contact the owner/author(s).

© 2020 Copyright held by the owner/author(s).

0730-0301/2020/7-ART1

<https://doi.org/10.1145/3386569.3392387>

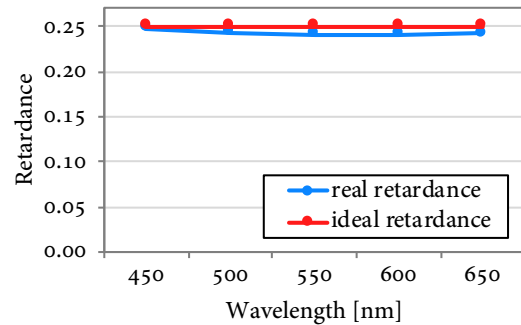


Fig. 1. Retardance of the employed achromatic retarder (Thorlabs AQWP10M-580). This quarter-wave retarder is designed to be achromatic, but the actual retardance values present a small deviation from the ideal value (0.25) across the visible wavelength, which is accounted by our linear reconstruction method.

## 3 PBRDF TABULATION

Once we reconstruct raw Mueller matrices of pBRDF, we transform these measurements into the Rusinkiewicz parameterization and discretize them into a 6D tensor, inspired by Matusik et al. [2003]. Its dimensions correspond to the half and difference angles  $\theta_h, \theta_d, \phi_d$ , wavelength  $\lambda$ , and the row and column of the Mueller matrix. The raw Mueller matrices of pBRDF are stored in the image space, and thus they are sampled to the parameterized tabulation across the light source positions. Here the mapping procedure is described in detail.

*Table specification.* Our pBRDF table  $T$  of a single material is formed as  $T(\lambda^i, \theta_h^j, \theta_d^k, \phi_d^l)$ , where  $\lambda^i, \theta_h^j, \theta_d^k, \phi_d^l$  indicate sampling wavelength and Rusinkiewicz angles corresponding to the table indices of  $i, j, k, l$ . Each bin of  $T$  stores a  $4 \times 4$  Mueller matrix. Rusinkiewicz coordinate system [Rusinkiewicz 1998] provide an efficient sampling strategy for tabulation by allowing dense sampling near specular highlight region [Matusik 2003]. We assign 91, 91, 361 bins for each of  $\theta_h, \theta_d, \phi_d$  indices respectively and they have the range of  $[0, \pi/2], [0, \pi/2], [-\pi, \pi]$ . Linear sampling is employed for  $\theta_d$  and  $\phi_d$  while we use quadratic sampling strategy for  $\theta_h$ :  $\theta_h^j = (j/91)^2 \times 90$  in degree, where  $j$  is the bin index. Our table also includes the spectral dimension with five bins obtained as we captured pBRDF with five narrow-band bandpass filters.

Item #	Part description	Quantity	Model name	Company
1	Machine vision camera	1	GS3-U3-91S6M	FLIR
2	Imaging lens	1	CoastalOpt apochromatic lens	Jenoptik
3	Light source	1	MCWHLP1	Thorlabs
4	Achromatic doublet	1	AC254-040-A-ML	Thorlabs
5	Automatic filter wheel	1	#59-769	Edmund Optics
6	Automatic turntable	1	Platinum MID turntable	Iconasys
7	Motorized rotary stage	2	K10CR1/M	Thorlabs
8	Manual rotary stage	2	RSP1	Thorlabs
9	Linear polarizer	2	#47-215	Edmund Optics
10	Quarter-wave retarder	2	AQWP10M-580	Thorlabs
11	Visible bandpass filter set	1	#88-299	Edmund Optics

Table 1. List of components for our pBRDF acquisition system.

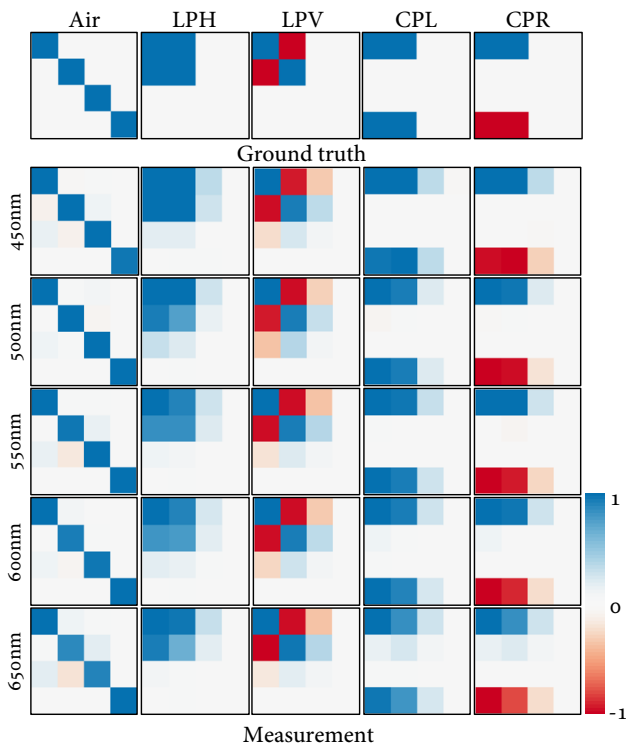


Fig. 2. We reconstruct the Mueller matrices of five basic elements compared with their ideal Mueller matrices in perfect orientation. From the left to the right, we show measurements of air, horizontal linear polarizer (LPH), vertical linear polarizer (LPV), left-hand circular polarizer (CPL), and right-hand circular polarizer (CPR). These Muller matrices are reconstructed by our Muller matrix reconstruction method.

*Calibrated values.* Through camera calibration, we obtained focal length and principal points of the camera system. Center of the camera (c) is at the origin of the camera coordinate system. The target sphere’s radius ( $r$ ) is manually measured. With the known radius, we compute the sphere center position (o) by detecting the sphere in the captured image under the ambient light condition. We denote  $l_c$  as the distance from the sphere center to the camera

center. We obtain the light source location (l) for every position of the rotating arm of the turntable. Then, we define the angle  $\theta_t$  as an angle between the vector ( $\vec{ol}$ ) from the sphere center to the light source and the vector ( $\vec{oc}$ ) from the sphere center to the camera. Angle  $\theta_t$  is associated with a specific light source position in our capture configuration by choosing the nearest one among our calibrated light positions.

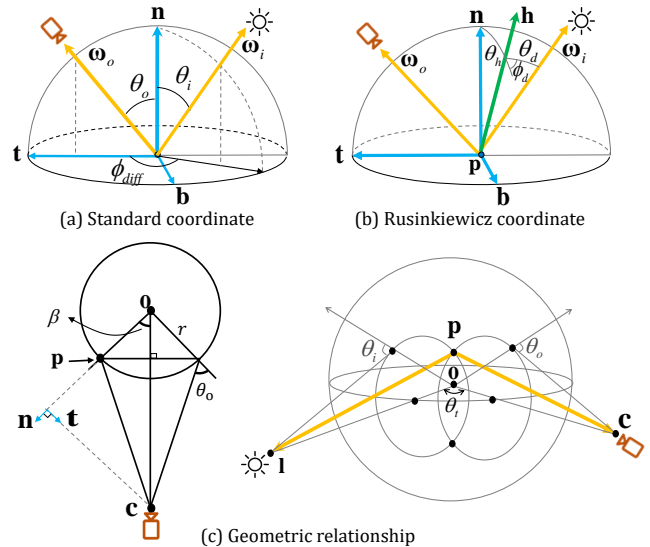


Fig. 3. This figure depicts the pBRDF model defined on (a) standard coordinates and (b) Rusinkiewicz coordinates at  $tnb$ -space. (c) visualizes the geometric relationship of the camera, object, and illumination.

*Light source location.* We captured images at different light source positions by rotating the illumination attached to the turntable. Given angles  $\theta_h, \theta_d, \phi_d$  corresponding to a pBRDF table indices  $i, j, k, l$ , we first need to identify the specific position of the light source, represented by  $\theta_t$ , which contains corresponding samples in our capture setup. To this end, we first convert the Rusinkiewicz coordinate to the standard coordinate angles  $\theta_i, \theta_o, \phi_{diff}$  (Figure 3).

$\omega_i$  and  $\omega_o$  indicate corresponding illumination vector and the view vector. We then locate the sample point on the sphere in the local *tbn* space:  $\mathbf{p}_{\text{tbn}} = [0, 0, 0, 1]$ . Sphere center in the *tbn* space is represented as  $\mathbf{o}_{\text{tbn}} = [0, 0, -r, 1]$ . We describe the light source position and the camera position also in the *tbn* space:  $\mathbf{l}_{\text{tbn}} = \mathbf{p}_{\text{tbn}} + \left[ \frac{\|\vec{\mathbf{l}}\|}{\|\vec{\mathbf{l}}\|_2} \omega_i, 0 \right]$  and  $\mathbf{c}_{\text{tbn}} = [l_c \sin \beta, 0, l_c \cos \beta, 1]$ , where  $\beta = \angle \mathbf{poc}$ . Finally, we compute the value of  $\theta_t$  as  $\angle \mathbf{c}_{\text{tbn}} \mathbf{o}_{\text{tbn}} \mathbf{l}_{\text{tbn}}$ . Once we obtain  $\theta_t$  for Rusinkiewicz coordinates of  $\theta_h, \theta_d, \phi_d$ , we finally can select a light-source location  $\theta$  in our setup having the most similar  $\theta_t$ .

*Pixel Sampling.* Since the light source position is identified, one remaining task is to locate the pixel location in the image space of having  $\theta_i$  and  $\theta_o$ . We first draw a circle so that the every surface point on the circle has the incident angle of  $\theta_i$ . Another circle is also made for the outgoing angle  $\theta_o$ . The intersection points of two circles therefore are the samples having  $\theta_i$  and  $\theta_o$ . We simply solve a quadratic equation for obtaining them. Located surface points are then projected to the image space with the calibrated camera parameters resulting in exact mapping between the pixel locations in the image domain to the pBRDF table indices of  $\theta_h, \theta_d, \phi_d$ . We use bilinear interpolation for sub-pixel sampling of pBRDF precomputed in the image domain.

#### 4 FITTING PBRDF MODELS

We compared our data-driven pBRDF models with two existing pBRDF models of Baek et al. [2018] and Hyde et al. [2009]. Since our pBRDF table per material amounts to 912 MiB, we downsampled the table by a factor of four in each of its directional dimension. For fitting, 16 different parameters of the pBRDF analytic models [Baek et al. 2018; Hyde IV et al. 2009] are used, which include one roughness value, and specular coefficient, diffuse albedo, and refractive index per each spectrum band. We used the sum of square root of the differences of  $4 \times 4$  pBRDF Mueller matrices as the cost function to be minimized by a nonlinear optimizer [Byrd et al. 2000].

#### REFERENCES

- Seung-Hwan Baek, Daniel S Jeon, Xin Tong, and Min H Kim. 2018. Simultaneous acquisition of polarimetric SVBRDF and normals. *ACM Trans. Graph.* 37, 6 (2018), 268–1.
- Richard H Byrd, Jean Charles Gilbert, and Jorge Nocedal. 2000. A trust region method based on interior point techniques for nonlinear programming. *Mathematical programming* 89, 1 (2000), 149–185.
- MW Hyde IV, JD Schmidt, and MJ Havrilla. 2009. A geometrical optics polarimetric bidirectional reflectance distribution function for dielectric and metallic surfaces. *Optics express* 17, 24 (2009), 22138–22153.
- Wojciech Matusik. 2003. *A data-driven reflectance model*. Ph.D. Dissertation. Massachusetts Institute of Technology.
- Szymon Rusinkiewicz. 1998. A New Change of Variables for Efficient BRDF Representation. In *Proc. Eurographics Rendering Workshop*. 11–22.